Performance of Self-Powered, Water-Resistant Bending Sensor Using Transverse Piezoelectric Effect of Polypropylene Ferroelectret Polymer

Yunqi Cao, *Student Member, IEEE*, Wei Li, and Nelson Sepúlveda, *Senior Member, IEEE*

***Abstract*— The significant growth of wearable electronics is in constant search for optimizing systems with high flexibility and self-powering capacity. In this work, we utilize flexible polypropylene ferroelectret (PPFE) thin film polymer with the large transverse piezoelectric coefficient for bending curvature self-powered sensing. The electric energy comes from the geometry distortion of the built-in macro dipoles with initial surface charge distributions. Theoretical analysis based on constitutive electromechanical equations and bi-layer bending mechanics provide a detailed understanding of the sensing mechanism and its applicability. Different evaluation methods are used to have a more comprehensive understanding of the electromechanical responses under different bending conditions. It has been found that the velocity and magnitude of the mechanical input influence the average voltage output, while instantaneous voltage is not dependent on the latter. The robustness of the material is also investigated, where the device shows no performance degradation by immersion into the water up to 12 hours and under 10k bending cycles. Thermal stability tests reveal degradation starting at ∼ 75°C and an immediate failure of the device at ∼ 150°C. Finally, an application is demonstrated by showing the potential use of the characterized system as a self-powered sensor for athletic assessment.**

***Index Terms*— Self-powered, bending sensor, ferroelectret, piezoelectric effect, waterproof, athletic assessment.**

I. Introduction

THE use of wearable electronics in human health is becoming more common in collecting physical data such as respiration rate [1], sleeping [2] and walking patterns [3], and even glucose levels [4]. This is achieved by using light, chemical, and acceleration sensors within a single device. Integrated with the Internet of Things (IoT) terminal devices such as smartphone or bracelet, the collected data provides critical information for long term health monitoring and pre-diagnosis analysis. The use of such wearable gadgets can be extended to include kinesiology-related information and perhaps allow for monitoring and improvement of athletic performance. Adding accurate information on the movement of specific body parts, while monitoring the athlete's health could lead to better overall assessment both in performance and health. Nevertheless, such devices need to meet the IoT system integration requirements in terms of size and weight, power consumption and robustness, etc.

Bending strain gauges are sensors that can play a major role in motion monitoring wearable gadgets, which can be used for detecting large deflections. Progresses in flexible electronics of making deformable, stretchable and biocompatible bending sensors also extend their integration in IoT systems. Conventional resistive strain sensors are usually based on metal foils and semiconductor coatings which utilize the resistance change due to geometrical effect. Limited by the low mechanical compliance, metal foil sensors only provide a detection range of 2% ∼ 5% [5]. Higher sensitivity can be achieved by utilizing microstructural disconnection mechanism in metallic nanomaterials, such as nanowire (AgNW) [6] and gold nanoparticle (AuNP) [7], coated on polymer substrates. Recent progress has also demonstrated fully elastomer-based resistive strain sensors based on carbon nanotube (CNT) [8], graphene [9], and laser scribing technique [10], etc. However, those passive sensors still require external power to translate the mechanical inputs to electric signals, e.g. a voltage divider circuit is required in resistive strain gauges. Therefore, it is contradictory to the requirement of IoT sensing networks which impose the sustainability and low power consumption on the sensing elements.

As an alternative option, piezoelectric materials with high sensitivity and self-powering capability have been exploited thoroughly in motion-sensing applications. Inorganic piezomaterials such as PZT [11], $BaTiO_3$ [12] and ZnO [13] can be deposited [14] onto or dispersed [15] into soft substrates such as polydimethylsiloxane (PDMS), polyethylene terephthalate (PET), etc. and high stretchability of up to ∼ 30% has been demonstrated [16]. However, the fabrication process is substrate-dependent or time consuming which presents a limitation in mass production for consumable electronic IoT systems. Electroactive polymer (EAP) offers great flexibility and stretchability, therefore can be mounted on nearly any surfaces (it is not substrate-dependent). The inherently low

Manuscript received June 26, 2019; revised August 1, 2019; accepted August 1, 2019. Date of publication August 2, 2019; date of current version October 17, 2019. This work was supported in part by the National Science Foundation under Grant ECCS-1854750, and in part by the MSU Strategic Partnership under Grant 16-SPG-Full-3236. The associate editor coordinating the review of this article and approving it for publication was Prof. Octavian Postolache. *(Corresponding author: Nelson Sepúlveda.)*

Y. Cao and N. Sepúlveda are with the Department of Electrical and Computer Engineering, Michigan State University, East Lansing, MI 48824 USA (e-mail: nelsons@egr.msu.edu).

W. Li is with the Department of Electrical Engineering and Computer Sciences, University of California, Berkeley, CA 94720 USA.

This article has supplementary downloadable material available at http://ieeexplore.ieee.org, provided by the author.

Digital Object Identifier 10.1109/JSEN.2019.2933174

piezoelectricity can be significantly optimized by nanotechnology and post-poling techniques [17]–[19].

Although EAPs exhibit similar piezoelectric effect, piezoelectricity can be introduced in materials in different ways including piezoelectric, triboelectric and ferroelectric. Piezoelectric sensors often utilize the piezoelectric effect of nanofibers [20], [21] when the device is being stretched or released. On the other hand, the transduction mechanism in triboelectric based bending sensors is attributed to the frictions caused by internal stress gradient [22], [23]. Ferroelectret EAP has been introduced as a relatively new type of transducer [24], the strong piezoelectric effect is introduced by precharging the internal engineered ellipsoid voids to form giant macro dipoles. Dynamic electromechanical behavior has been investigated mainly under compressive loads [25]–[28], and applications include energy harvesters [29], [30], loudspeakers [31], and pressure sensors [32], [33], etc. But potential applications as bending sensors still need to be exploited. Despite all those continuous efforts that have been made to improve the device performance, little attention has been paid to the evaluation methods - i.e. instantaneous voltage peak outputs are usually measured for the device characterization and motion calibration. However, dynamic information could be missed for specific bending operations and therefore a more comprehensive evaluation method is required.

In this article, we present the characterization of a flexible ferroelectret polypropylene (PP) polymer film with a strong piezoelectric effect as a wearable bending self-powered sensor, including its performance under different conditions and environments. The relations between electrical outputs (current and voltage) and bending conditions are developed from the fundamental governing equations that describe general piezoelectric behavior and a bi-layer bending model. The piezoelectric effect under the bending operation is originated from the transverse piezoelectric coefficient [34] which leads to a decrease in the dipole separation distance under axial compression. Different evaluation methods are used for bending monitoring in terms of peak and average values of the voltage and current outputs respectively, and therefore different bending information can be extracted and evaluated. The developed equations predict the electromechanical behavior and determine the dominating parameters in characterizing the electrical outputs for this engineered EAP material. Mechanical robustness, thermal and humidity stabilities are also demonstrated in this work. Finally, the acquired models are implemented in an athletic monitoring system, based on the comparison of generated electric waveforms.

II. Materials and Experimental Methods

Polypropylene ferroelectret film is an EAP material with piezoelectric properties. The material consists of two continuous surfaces of PP film, and is porous across its thickness, as shown in the inset in Fig.1a. The macro-scale ellipsoid air voids are created by an in-plane two-directional stretching process with the help of silica particles as stress concentrators. Nitrogen gas is then introduced with a high-pressure atmosphere to allow N_2 molecules diffuse into the voids,

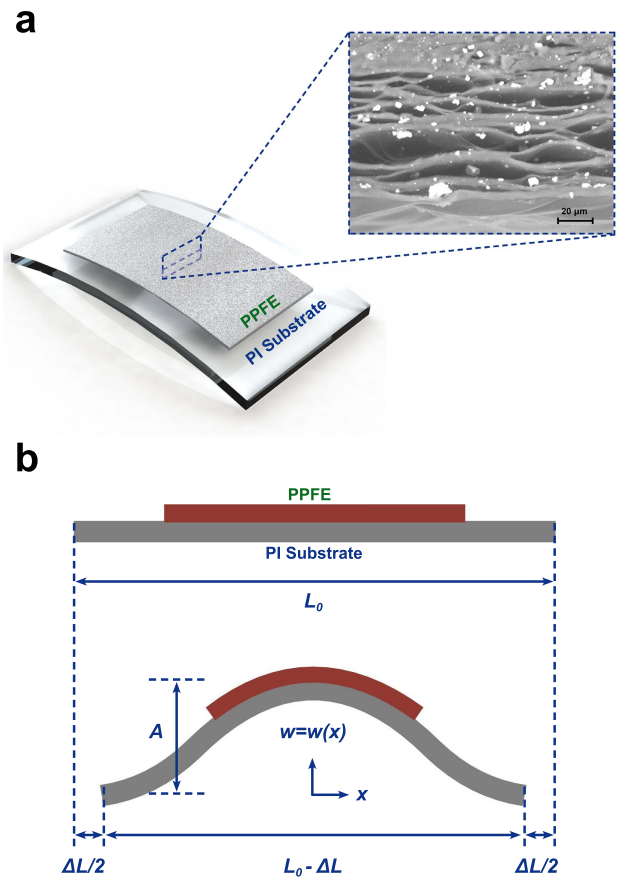

Fig. 1. Bending configuration of PPFE thin film mounted on a flexible PI substrate. (a) 3D schematic drawing of silver coated PPFE film mounted on PI substrate, inset shows the SEM image of the cross section view of PPFE film. (b) 2D Schematic diagram of a sinusoidal shape buckling profile under a horizontal axial compression displacement.

and a sudden release of the high-pressure environment is followed in order to trap the N_2 gas and expand the voids into an ellipsoid shape. A high electric field is then applied to create plasma discharging, resulting in electric charges with opposite polarities trapped on both surfaces of the voids. Each charged void can be considered as a macro scaled dipole with a permanent dipole moment. Mechanical loads that cause structural distortion of the dipole would lead to changes in the displacement field inside the material. Therefore displacement current is generated which realizes the transduction from the mechanical to the electrical domain. The porous structure significantly increases the compliance of the material (Young's Modulus: $E < 10^6\ Pa$ [35] compared to solid PP film with $E = 1.5 \times 10^9 \sim 2 \times 10^9\ Pa$) which translates into excellent flexibility for soft electronics and their human interface. Here, we focus on the distortion of the macro dipoles and the consequent electric output under a bending operation caused by an axial displacement. As shown in Fig.1a, the PPFE film is attached to a flexible PI substrate. In this configuration, the electromechanical response can be described by characterizing the output voltage/current to the generated deflection due to an axial load that results in a buckled bridge shape shown in Fig.1b. The experiment is assisted by using a computer-controlled stepper motor as the linear actuator to

provide the horizontal compressive axial stress that causes axial displacement ΔL and vertical displacement w. In order to compare different electromechanical responses under different bending conditions, ΔL and the compression velocity v were programmed by pulse width modulation (PWM) of DC voltages applied to the motor.

III. Results and Discussion

Assuming the initial length of the PI substrate is L_0, the flexible sample buckles into a sinusoidal shape with w described as a function of horizontal axial parameter x as: $w(x) = A[1 + cos(2\pi x/L_0)]/2$, where the origin of x is at the center and A is the maximum buckling amplitude given by $A = (2/\pi)\sqrt{L_0 \Delta L}$ [36]. The in-plane x-axial strain (ϵ_{11}) within the PPFE can be estimated by using the curvature of the buckled shape as: $\epsilon_{11} = -w''(x)(h_{PPFE} + h_{PI})/2$, where $w''(x)$ is the bending curvature, h_{PPFE} is the thickness of PPFE film and h_{PI} is the thickness of the PI substrate. Given that the PPFE film is located at the center of the PI substrate where maximum longitudinal strain occurs, ϵ_{11} can be approximated as:

$$\epsilon_{11} = \frac{2\pi(h_{PPFE} + h_{PI})\sqrt{\Delta L}}{L_0\sqrt{L_0}}, \tag{1}$$

from which we can use the fundamental equations that relate strain to the electric field in piezoelectric materials (see Supporting Information for details) to obtain:

$$V_{oc} = \frac{2\pi(h_{PPFE} + h_{PI})\overline{d}h_{PPFE}}{\overline{k}L_0\sqrt{L_0}}\sqrt{\Delta L}, \tag{2}$$

where $\overline{d} = d_{33}c_{12}/c_{13} - d_{31}$ and $\overline{k} = k_{33} + d_{33}d_{31}/c_{13}$, d_{33}, c_{12}, c_{13}, d_{31} and k_{33} come from piezoelectric matrix and stress/strain transformation matrix (see Supporting Information for details). Thus, V_{oc} is proportional to the strain in PPFE film which is exactly the linear coupling relation between mechanical and electrical properties in piezoelectric materials.

However, V_{oc} measurements are often taken by connecting a voltmeter across the open circuit terminals at the output of the device [37]. Therefore, the profile of the measured V_{oc} will be dependent on the instrument's internal resistance; and its proximity to a real open-circuit scenario will increase with this internal resistance value. In this work, a Keithley 2450 is used to measure V_{oc}, which has an internal resistance $\geq$ 10 GΩ. Fig.2 shows the relation between ΔL, ϵ_{11}, and V_{oc}. The bidirectional linear axial displacement provided by stepper motor as shown in Fig.2a gives a normalized strain profile determined by Eq.(1) as shown in Fig.2b. The measured V_{oc} also shows a similar profile as ϵ_{11} which is also indicated by Eq.(2). Fig.2d shows the measured peak value of V_{oc} (scattered points) as a function of different maximum axial displacement ΔL_{max}, and the theoretical curve for these V_{oc} maximum points, taken from evaluating Eq.(2) at $\Delta L = \Delta L_{max}$.

For short circuit current measurements, the device is connected to an ammeter, where the voltage drop across is minimal. This results in a simple linear relation between displacement field D_3 and ϵ_{11} (see Supporting Information for details). Given that $I_{sc} = -S_{PPFE}(\partial D_3/\partial t)$, (where I_{sc} is the short circuit current and S_{PPFE} is the area of PPFE film), I_{sc} can be further expressed as (see Supporting Information for details):

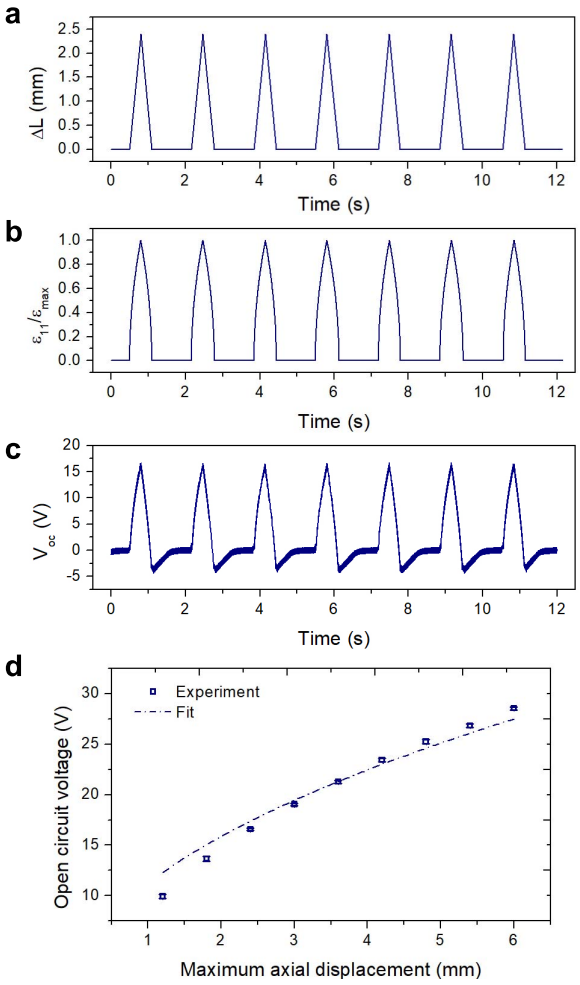

Fig. 2. Measured electrical response due to axial displacement ΔL and film strain ϵ_{11}. (a) Profile of linear axial compression displacement ΔL as a function of time. (b) Theoretical normalized film strain ϵ_{11} from Eq.(1) as a function of time. (c) Measured V_{oc} as a function of time. (d) Peak V_{oc} value as a function of ΔL_{max} for a given compression velocity of 14 mm/s.

$$I_{sc} = \frac{\pi\overline{d}S_{PPFE}(h_{PPFE} + h_{PI})}{L_0\sqrt{L_0}\sqrt{\Delta L}}\frac{d\Delta L}{dt}. \tag{3}$$

Eq.(3) shows that I_{sc} is proportional to the changing rate of compressive load ($\frac{d\Delta L}{dt}$), and its magnitude increases with PPFE film area; which can be achieved by stacking multiple layers or connecting them in parallel. For linear axial compression, the compression displacement can be described by the compression velocity v (input parameter) as:

$$\Delta L = \begin{cases} vt & \text{if } t < T/2 \\ v(T - t) & \text{if } T/2 < t < T, \end{cases} \tag{4}$$

where T is the time period for a complete compressing and releasing cycle. Thus, $I_{sc}(t)$ can be determined as:

$$I_{sc}(t) = \frac{\pi\overline{d}S_{PPFE}(h_{PPFE} + h_{PI})\sqrt{v}}{L_0\sqrt{L_0}}t^{-\frac{1}{2}} \tag{5}$$

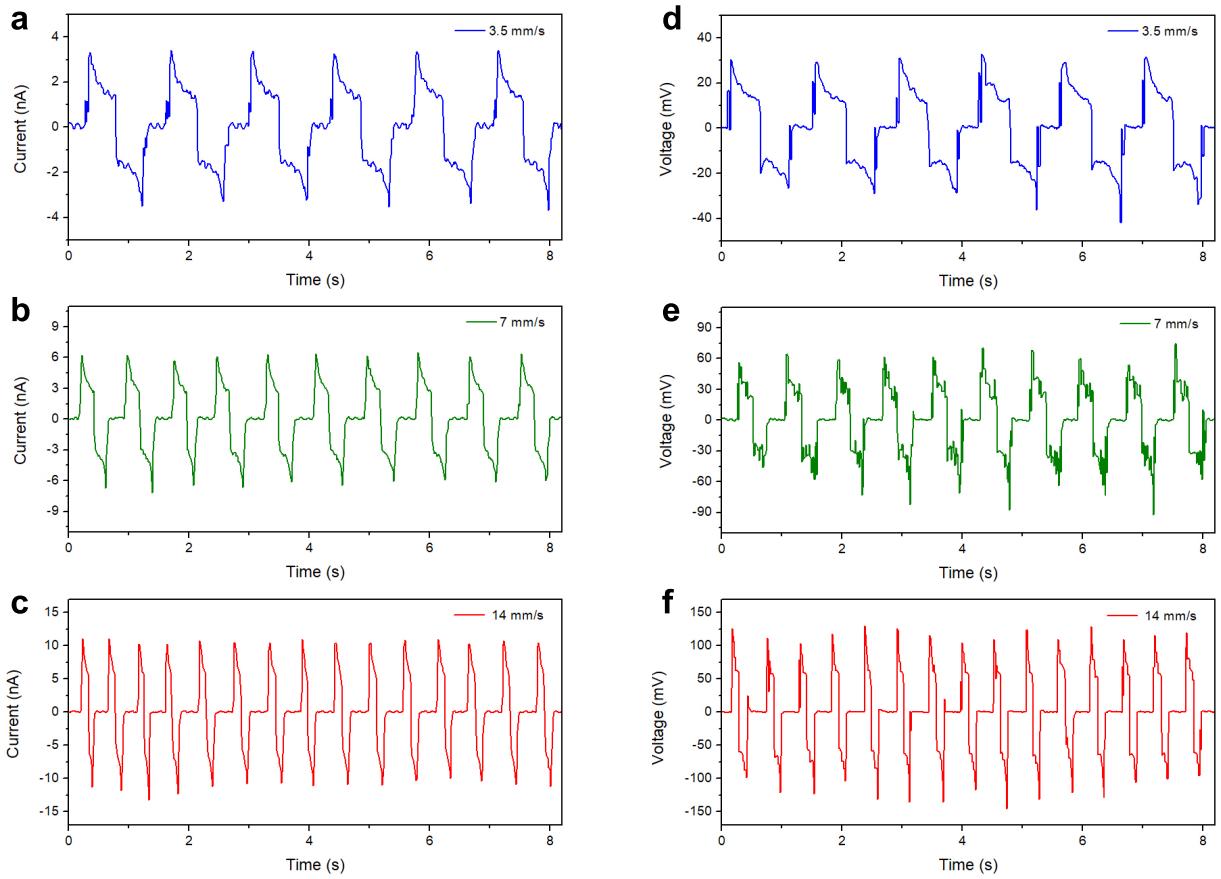

Fig. 3. Characterization of electrical output under bending test. (a,b,c) Short circuit current I_{sc} under the same $\Delta L_{max} = 3\ mm$ and different υ. From top to bottom: 3.5 mm/s, 7mm/s, and 14 mm/s. (d,e,f) Voltage measurement under the same $\Delta L_{max} = 3\ mm$ and different υ, from top to bottom: 3.5 mm/s, 7 mm/s, and 14 mm/s.

for the compression stage. Eq.(5) indicates that the short circuit current increases with increasing υ, which is also shown in Fig.3a-c. The PPFE acts as a current transducer, which translates energy from the mechanical to the electrical domain. Therefore, the internal resistance R of the voltage measuring instrument must be taken into consideration. To distinguish the voltage measured by a voltmeter with low input impedance from the V_{oc} measured by an instrument with high input impedance, the symbol V is used for the clarity. In this case, the current flowing through the device-instrument circuit loop is also affected by R through the induction of an electric field. Thus, the measured voltage V can be determined by solving the differential equation (see Supporting Information). When the internal resistance of the voltmeter is much lower than the impedance of PPFE, V can be approximated to:

$$V \approx I_{sc} R, \tag{6}$$

where $R = 10\ M\Omega$ for the voltmeter Keithley 2182A used in this work. Therefore, voltage measurements (Fig.3d-f) have the same curve profile as I_{sc} (Fig.3a-c).

The characterization is performed for a PPFE film mounted on a PI substrate under axial stress that generates buckling (and bending), while the current and voltage are measured across the device. The axial compressive displacement is provided by a stepper motor with bi-directional displacement. The PPFE used for the bending test is 15 mm wide, 50 mm long, and 80 μm thick. Two 500 nm silver thin films are sputtered on both sides of the PPFE as electrodes. The device is mounted on a 25 mm $\times$ 60 mm PI substrate with a thickness of 0.8 mm. The ΔL_{max} and υ are programmed and controlled through the FPGA interface. Fig.3a-c show the measured I_{sc} under different compression velocities with the same maximum compression displacement of 3 mm, which is converted to curvature of 46.8 m^{-1}. As predicted by Eq.(5), the current output increases with increasing compression velocity. Fig.3d-f show the measured output voltage V under the same conditions used for measuring I_{sc}. The voltage output follows a similar relation with compression velocity to the one observed in I_{sc} measurements; which agrees with the described theory.

Characterizing self-powered sensors is often done in terms of peak short circuit current (I_{sc-max}) and measured peak voltage (V_{max}) values [38]. However, since I_{sc} is proportional to $t^{-\frac{1}{2}}$, the I_{sc-max} and V_{max} are found at $t = 0$ for any applied axial stress. This means that the largest generated electrical output occurs at the moment an axial displacement begins to occur; and therefore, I_{sc-max} and V_{max} should be independent of the maximum range of axial displacement, ΔL_{max}. This usually goes unnoticed, because for a commonly used bending condition, the ΔL_{max} is always coupled with a faster compression velocity υ; e.g. when ΔL_{max} is

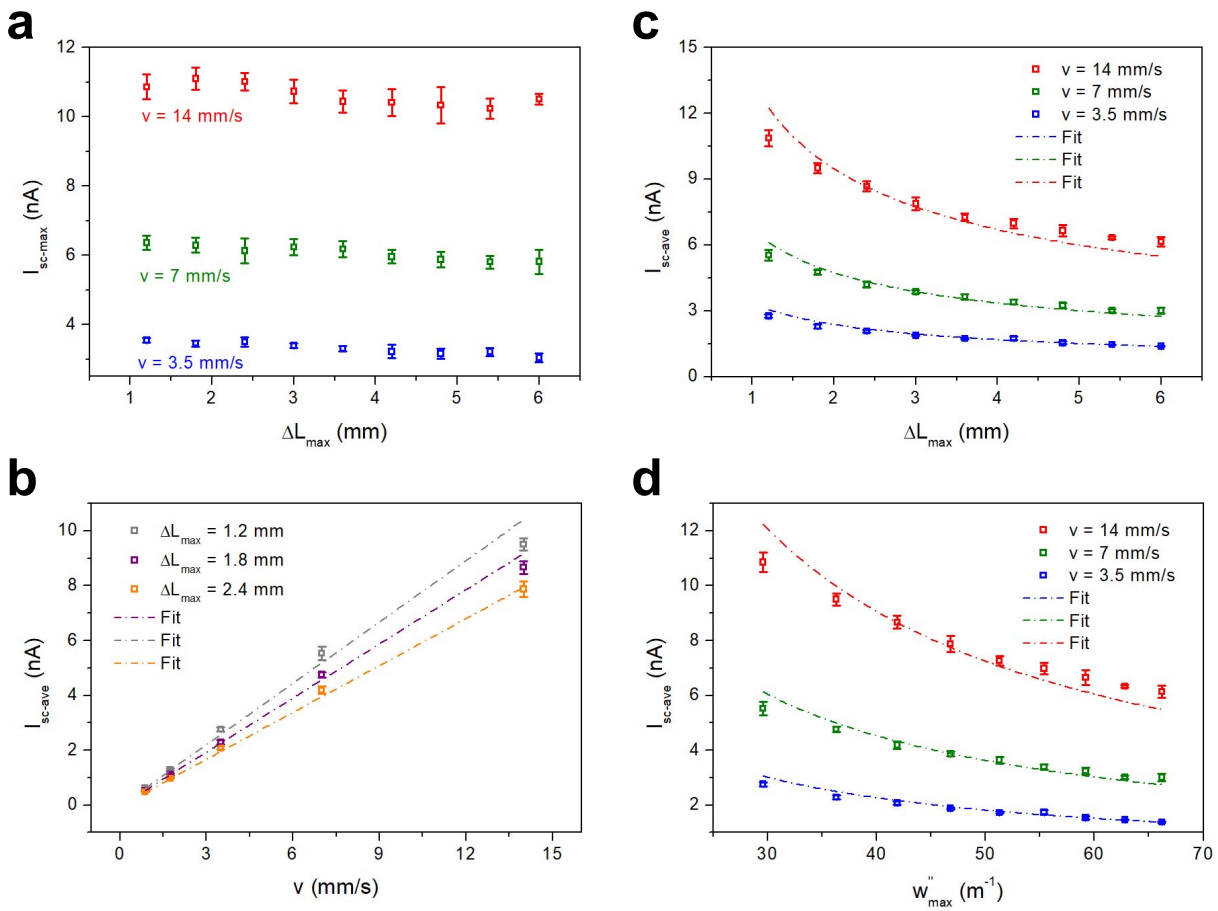

Fig. 4. Characterization of I_{sc-max} and I_{sc-ave} under bending test. (a) I_{sc-max} as a function of ΔL_{max} under different υ. (b) I_{sc-ave} as a function of υ under different ΔL_{max}. (c) I_{sc-ave} as a function of ΔL_{max} under different υ. (d) I_{sc-ave} as a function of w''_{max} under different υ. The fit curves are obtained from Eq.(7) by using proportional constants that best fit the measured data.

increased, the compression time period $T/2$ is kept the same, leading to a higher υ.

The relation between the maximum instantaneous current and voltage output is further characterized by using different compression velocities and axial displacements (or curvatures). Fig.4a shows the I_{sc-max} under different axial displacement velocities ranging from 3.5 mm/s to 14 mm/s with different maximum axial displacements from 1.2 mm to 6 mm, which converts to a bending curvature range of 29.6 m^{-1} to 66.2 m^{-1}. No obvious changes in I_{sc} and V_{oc} are observed for different ΔL_{max} under the same compression velocity, indicating that the compression velocity is the dominant factor in determining the peak electrical outputs under the bending operation. An estimation of the peak value can be made from Eq.(3) by giving a certain small (nonzero) time –usually determined by the instrument's sampling rate– and assuming the traveled distances in this time are comparable for different velocities. Then, the I_{sc-max} can be approximated to be linearly proportional to υ, which is also indicated in Fig.4a.

As indicated by Eq.(5) and Fig.3, the I_{sc-max} and V_{max} values are found at the beginning of each compression and releasing cycle, then decaying as a function of $t^{-\frac{1}{2}}$. For a compression stage, the average current output, I_{sc-ave}, can be calculated by averaging I_{sc} over the compression time period $T/2$, leading to:

$$I_{sc-ave} = \frac{\int_0^{\frac{T}{2}} I_{sc}dt}{T/2} = \frac{2\sqrt{2}\pi \overline{d} S_{PPFE}(h_{PPFE}+h_{PI})\upsilon}{L_0\sqrt{L_0\Delta L_{max}}}. \quad (7)$$

Eq.(7) gives the relation among I_{sc-ave}, υ, and ΔL_{max}. Fig.4b shows that I_{sc-ave} is linearly proportional to υ for each given ΔL_{max}, which is in agreement with the theory. Fig.4c shows measurements of I_{sc-ave} as a function of ΔL_{max} for different values of υ, where the data follows the square-root dependence on ΔL_{max} predicted by theory. For real application and bending sensing purposes, it is important to know the relation between the measured electric signal (I_{sc-ave} in this case) and bending curvature. Given that w'' is linearly proportional to ϵ_{11}, which is also linearly proportional to $\sqrt{\Delta L}$, I_{sc-ave} also exhibits an inverse dependence on w''_{max}, as shown in Fig.4d.

Given that most of the data acquisition and readout circuits are designed to respond to voltage signals, it is more desirable to have sensors that generate voltage output signals (instead of current signals). Typical commercial voltmeters have internal

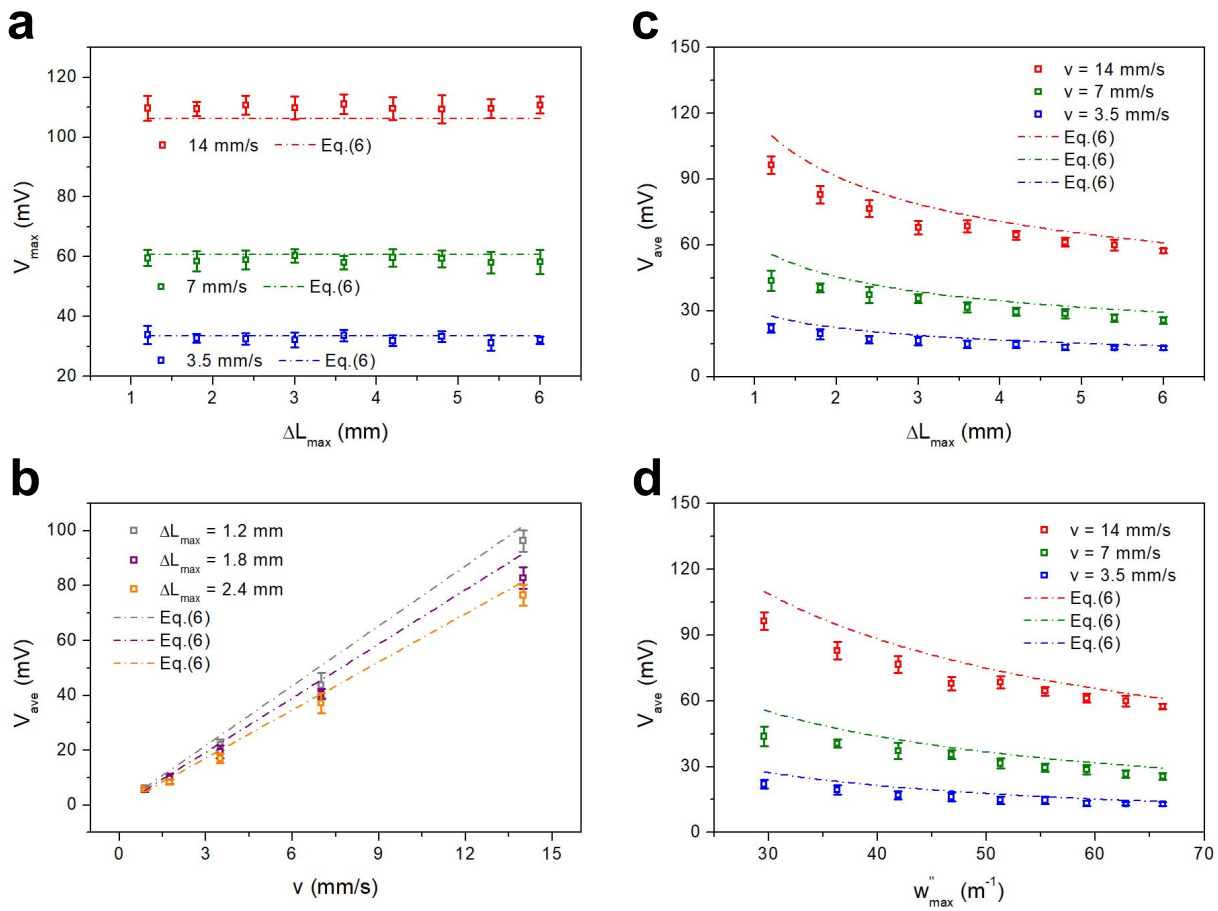

Fig. 5. Characterization of V_{max} and V_{ave} under bending test. (a) V_{max} as a function of ΔL_{max} under different υ. (b) V_{ave} as a function of υ under different ΔL_{max}. (c) V_{ave} as a function of ΔL_{max} under different υ. (d) V_{ave} as a function of w''_{max} under different υ.

resistances between 1 MΩ to 10 MΩ, which are much lower than the impedance of PPFE. Therefore, in the interest of completing a study that makes the proposed bending sensor more compatible with typical measuring instruments, the rest of the work is focused on the measured voltage V, instead of the ideal V_{oc} value. As discussed above, V can be approximated as $I_{sc}R$, and it is expected to exhibit similar dynamic profile as I_{sc}; which is observed experimentally (Fig.5). It should be noted that V_{oc} (Fig.2c) shows a different dynamic profile than V (Fig.3d-f), and the relationship between I_{sc} and V through the instrument's internal resistance ($V = I_{sc}R$) is validated in the experimental results shown in Fig.4 and Fig.5.

A study on the degradation of PPFE films in terms of mechanical robustness, resistance to humidity and thermal stability is performed next. Fig.6a shows the performance of PPFE as a function of bending cycles for an axial compression velocity of 14 mm/s and maximum bending curvature of 46.8 m^{-1}. This experiment was carried out using the same setup described for all the previous bending experiments. No significant degradation is observed during the repeated cycling test, indicating the PPFE film as a bending sensor exhibits long term mechanical stability.

Wearable sensors can be implemented in systems that allow for the assessment of an athlete's performance in sports. However, there are several factors that can deteriorate the device's reliability. For example, resistance to humidity is a key parameter which could significantly reduce the performance of the sensor, especially for those have the capacitive impedance. Triboelectric sensors with an air gap will experience a change in their performance due to the absorption of the ambient water and therefore require additional packaging methods [39]–[41]. Even tough PPFE has a porous structure, it is sandwiched in between two continuous PPFE films, which prevent the swelling of the voids due to water absorption. Thus, it proves to be water-resistant as demonstrated in Fig.6b. When using polymer as the base material for piezoelectric applications, the structure of the polymer may experience poor thermal stability. Fig.6c shows the performance percentage under different baking temperatures as a function of time. No degradation is observed for a baking temperature of 50°C. As the temperature increases, the material starts to degrade. When baked at 75°C, no degradation is measured until baking for 60 min, the performance saturates at the level of around 65%. Significant degradation appears at the temperature of 125°C and above. For a short time and low-temperature processes such as encapsulating PPFE into PDMS and PI layers, it is acceptable to sacrifice some of the performance. However, higher temperatures should be avoided, since

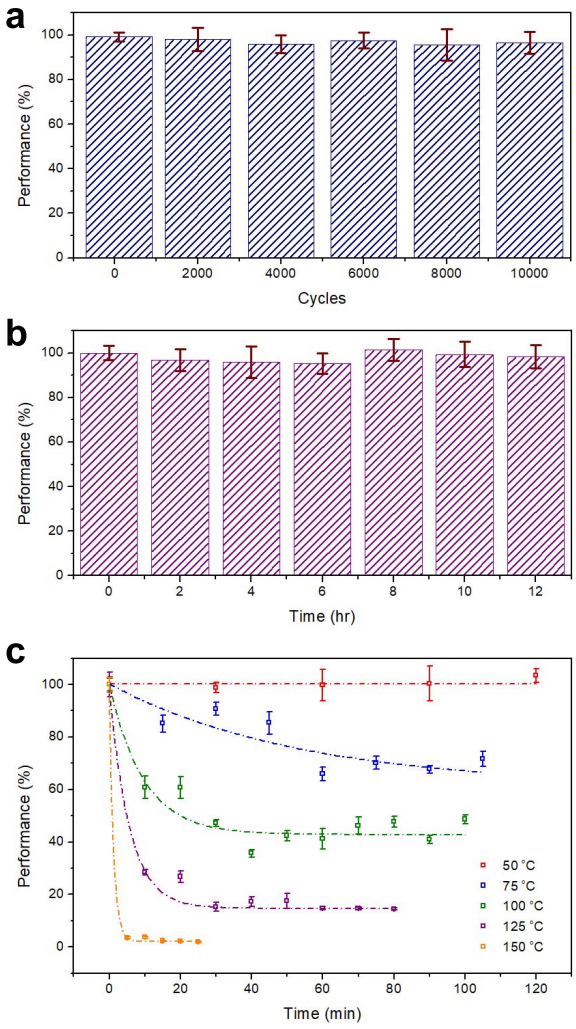

Fig. 6. Demonstration of performance degradation under different testing conditions. (a) Test of mechanical robustness under repeated bending cycling up to 10000 bending and releasing operations. (b) Test of humidity resistance by immersion into water for up to 12 hours. (c) Test of thermal stability under different baking temperatures.

a temperature of 150°C would destroy the quasi-piezoelectric property of the material due to the collapsing of the voided structure as shown in the Supporting Information.

Based on the analysis above, it can be seen that V_{max} and V_{ave} exhibit different behaviors under the same bending condition. This suggests that by monitoring these two parameters, information about the bending curvature and speed can be extracted. A potential application for this can be found in monitoring the bending curvature and speed of an athlete's wrist during a baseball throw or a basketball shoot. Hence, this flexible self-powered PPFE bending sensor can be attached to the player's wrist to monitor the posture and movement profile when participating in those sports. In the present application, we suggest a way to compare the bending profile of an athlete with what can be considered an "ideal movement behavior"; perhaps coming from a coach or a database that holds a history of "good throws". Fig.7a shows a demonstration of throwing a baseball from the player. Fig.7b and Fig.7c show

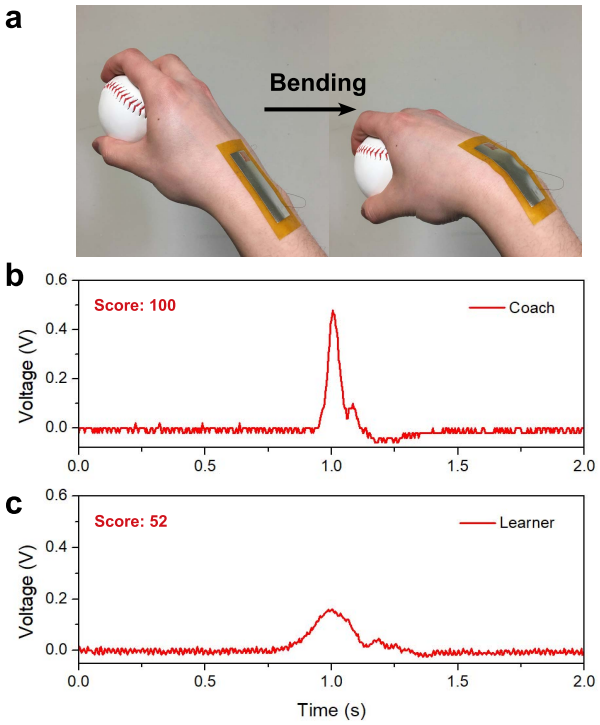

Fig. 7. Demonstration of application in the athletic assessment. (a) Photography of showing bending of the wrist during throwing a baseball. (b) Voltage output signal from the coach throwing the baseball. (c) Voltage output signal from the learner throwing the baseball.

the measured voltage waveforms from a coach and the athlete, respectively. By comparing the V_{max} and V_{ave} values obtained by the coach and the athlete, a learning score can be generated from the algorithm described in the Supporting Information. This way, the athlete can monitor his/her athletic performance and even have a database with a history of the progress made.

IV. Conclusion

The porous flexible polypropylene ferroelectret (PPFE) thin film is introduced in this work as a bending sensor. The bending operation is provided by an axial displacement and the bending profile follows the fundamental mechanical analysis. The outputs of PPFE film in terms of open circuit voltage, short circuit current, and measured voltage are characterized under different bending conditions. Given that the PPFE can be considered as a current source with large internal impedance, its voltage measurement is heavily dependent on the internal resistance of the voltage measurement instrument. To clarify the bending dependency of an electric output, I_{sc-ave} and V_{ave} are used instead of I_{sc-max} and V_{max}. The average electric output values are found to have a similar behavior due to the approximation under a condition of using low internal resistance voltmeter. Both outputs show linear dependency on υ and inverse square-root dependency on w''_{max}. The robustness of the material in terms of bending repeatability, resistance to humidity, and thermal stability are also presented for considerations in real applications, such as the sports assessment application demonstrated in this work.

ACKNOWLEDGMENT

The authors would like to thank the Center for Advanced Microscopy (CAM) at Michigan State University.

REFERENCES

[1] L. Wang and K. J. Loh, "Wearable carbon nanotube-based fabric sensors for monitoring human physiological performance," *Smart Mater. Struct.*, vol. 26, no. 5, Apr. 2017, Art. no. 055018.

[2] X. Ding, H. Cao, X. Zhang, M. Li, and Y. Liu, "Large scale triboelectric nanogenerator and self-powered flexible sensor for human sleep monitoring," *Sensors*, vol. 18, no. 6, p. 1713, May 2018.

[3] M. S. Rasel *et al.*, "An impedance tunable and highly efficient triboelectric nanogenerator for large-scale, ultra-sensitive pressure sensing applications," *Nano Energy*, vol. 49, pp. 603–613, Jul. 2018.

[4] H. Lee, Y. J. Hong, S. Baik, T. Hyeon, and D.-H. Kim, "Enzyme-based glucose sensor: From invasive to wearable device," *Adv. Healthcare Mater.*, vol. 7, no. 8, Apr. 2018, Art. no. 1701150.

[5] L. Cai *et al.*, "Super-stretchable, transparent carbon nanotube-based capacitive strain sensors for human motion detection," *Sci. Rep.*, vol. 3, p. 3048, Oct. 2013.

[6] S. Chen, Y. Wei, S. Wei, Y. Lin, and L. Liu, "Ultrasensitive cracking-assisted strain sensors based on silver nanowires/graphene hybrid particles," *ACS Appl. Mater. Interfaces*, vol. 8, no. 38, pp. 25563–25570, Sep. 2016.

[7] X. Liao, Z. Zhang, Q. Liang, Q. Liao, and Y. Zhang, "Flexible, cuttable, and self-waterproof bending strain sensors using microcracked gold nanofilms paper substrate," *ACS Appl. Mater. Interfaces*, vol. 9, no. 4, pp. 4151–4158, Jan. 2017.

[8] L. Wang *et al.*, "Highly stretchable, anti-corrosive and wearable strain sensors based on the PDMS/CNTs decorated elastomer nanofiber composite," *Chem. Eng. J.*, vol. 362, pp. 89–98, Apr. 2019.

[9] Z. Yang *et al.*, "Graphene textile strain sensor with negative resistance variation for human motion detection," *ACS Nano*, vol. 12, no. 9, pp. 9134–9141, Aug. 2018.

[10] Y. Zhu, H. Cai, H. Ding, N. Pan, and X. Wang, "Fabrication of low-cost and highly sensitive graphene-based pressure sensors by direct laser scribing polydimethylsiloxane," *ACS Appl. Mater. Interfaces*, vol. 11, no. 6, pp. 6195–6200, Jan. 2019.

[11] G.-T. Hwang *et al.*, "Self-powered wireless sensor node enabled by an aerosol-deposited PZT flexible energy harvester," *Adv. Energy Mater.*, vol. 6, no. 13, Jul. 2016, Art. no. 1600237.

[12] S.-H. Shin, Y.-H. Kim, M. H. Lee, J.-Y. Jung, and J. Nah, "Hemispherically aggregated $BaTiO_3$ nanoparticle composite thin film for high-performance flexible piezoelectric nanogenerator," *Acs Nano*, vol. 8, no. 3, pp. 2766–2773, Feb. 2014.

[13] Y. Qiu *et al.*, "Flexible piezoelectric nanogenerators based on ZnO nanorods grown on common paper substrates," *Nanoscale*, vol. 4, no. 20, pp. 6568–6573, Aug. 2012.

[14] J. Akedo and M. Lebedev, "Microstructure and electrical properties of lead zirconate titanate ($Pb(Zr_{52}/Ti_{48})O_3$) thick films deposited by aerosol deposition method," *Jpn. J. Appl. Phys.*, vol. 38, no. 9S, p. 5397, Sep. 1999.

[15] D. B. Deutz, N. T. Mascarenhas, J. Ben J. Schelen, D. M. de Leeuw, S. van der Zwaag, and P. Groen, "Flexible piezoelectric touch sensor by alignment of lead-free alkaline niobate microcubes in PDMS," *Adv. Funct. Mater.*, vol. 27, no. 24, Jun. 2017, Art. no. 1700728.

[16] X. Niu *et al.*, "High-performance PZT-based stretchable piezoelectric nanogenerator," *ACS Sustain. Chem. Eng.*, vol. 7, no. 1, pp. 979–985, Dec. 2018.

[17] P. Zhao *et al.*, "Emulsion electrospinning of polytetrafluoroethylene (PTFE) nanofibrous membranes for high-performance triboelectric nanogenerators," *ACS Appl. Mater. Interfaces*, vol. 10, no. 6, pp. 5880–5891, Jan. 2018.

[18] H. Kim, F. Torres, Y. Wu, D. Villagran, Y. Lin, and T.-L. B. Tseng, "Integrated 3D printing and corona poling process of PVDF piezoelectric films for pressure sensor application," *Smart Mater. Struct.*, vol. 26, no. 8, Jul. 2017, Art. no. 085027.

[19] J. Ouyang, D. Cormier, and D. A. Borkholder, "Piezoelectric property enhancement of PZT thick film via pulsed flash poling during sintering," *ACS Appl. Energy Mater.*, vol. 2, no. 1, pp. 338–343, Dec. 2018.

[20] G. Zhao *et al.*, "Piezoelectric polyacrylonitrile nanofiber film-based dual-function self-powered flexible sensor," *ACS Appl. Mater. Interfaces*, vol. 10, no. 18, pp. 15855–15863, Apr. 2018.

[21] K. Maity and D. Mandal, "All-organic high-performance piezoelectric nanogenerator with multilayer assembled electrospun nanofiber mats for self-powered multifunctional sensors," *ACS Appl. Mater. Interfaces*, vol. 10, no. 21, pp. 18257–18269, May 2018.

[22] F.-R. Fan, L. Lin, G. Zhu, W. Wu, R. Zhang, and Z. L. Wang, "Transparent triboelectric nanogenerators and self-powered pressure sensors based on micropatterned plastic films," *Nano Lett.*, vol. 12, no. 6, pp. 3109–3114, May 2012.

[23] S. Lee *et al.*, "Triboelectric energy harvester based on wearable textile platforms employing various surface morphologies," *Nano Energy*, vol. 12, pp. 410–418, Mar. 2015.

[24] S. K. Ghosh, T. K. Sinha, B. Mahanty, and D. Mandal, "Self-poled efficient flexible 'ferroelectretic' nanogenerator: A new class of piezoelectric energy harvester," *Energy Technol.*, vol. 3, no. 12, pp. 1190–1197, Dec. 2015.

[25] Z. Luo *et al.*, "Energy harvesting study on single and multilayer ferroelectret foams under compressive force," *IEEE Trans. Dielectr. Electr. Insul.*, vol. 22, no. 3, pp. 1360–1368, Jun. 2015.

[26] X. Zhang, G. M. Sessler, and Y. Wang, "Fluoroethylenepropylene ferroelectret films with cross-tunnel structure for piezoelectric transducers and micro energy harvesters," *J. Appl. Phys.*, vol. 116, no. 7, Aug. 2014, Art. no. 074109.

[27] J. Shi, S. Yong, and S. Beeby, "An easy to assemble ferroelectret for human body energy harvesting," *Smart Mater. Struct.*, vol. 27, no. 8, Jul. 2018, Art. no. 084005.

[28] S. Rajala, M. Paajanen, and J. Lekkala, "Measurement of sensitivity distribution map of a ferroelectret polymer film," *IEEE Sensors J.*, vol. 16, no. 23, pp. 8517–8522, Dec. 2016.

[29] W. Li, D. Torres, T. Wang, C. Wang, and N. Sepúlveda, "Flexible and biocompatible polypropylene ferroelectret nanogenerator (FENG): On the path toward wearable devices powered by human motion," *Nano Energy*, vol. 30, pp. 649–657, Dec. 2016.

[30] Y. Cao *et al.*, "Flexible ferroelectret polymer for self-powering devices and energy storage systems," *ACS Appl. Mater. Interfaces*, vol. 11, no. 19, pp. 17400–17409, Apr. 2019.

[31] W. Li *et al.*, "Nanogenerator-based dual-functional and self-powered thin patch loudspeaker or microphone for flexible electronics," *Nature Commun.*, vol. 8, May 2017, Art. no. 15310.

[32] Y. Cao *et al.*, "Impact-activated programming of electro-mechanical resonators through ferroelectret nanogenerator (FENG) and vanadium dioxide," *Nano Energy*, vol. 43, pp. 278–284, Jan. 2018.

[33] I. Graz *et al.*, "Flexible ferroelectret field-effect transistor for large-area sensor skins and microphones," *Appl. Phys. Lett.*, vol. 89, no. 7, Aug. 2006, Art. no. 073501.

[34] X. Zhang, P. Pondrom, G. M. Sessler, and X. Ma, "Ferroelectret nanogenerator with large transverse piezoelectric activity," *Nano Energy*, vol. 50, pp. 52–61, Aug. 2018.

[35] Z. Luo, D. Zhu, and S. Beeby, "An electromechanical model of ferroelectret for energy harvesting," *Smart Mater. Struct.*, vol. 25, no. 4, Mar. 2016, Art. no. 045010.

[36] J. Song *et al.*, "Mechanics of noncoplanar mesh design for stretchable electronic circuits," *J. Appl. Phys.*, vol. 105, no. 12, Jun. 2009, Art. no. 123516.

[37] Y. Cao, J. Figueroa, W. Li, Z. Chen, Z. L. Wang, and N. Sepúlveda, "Understanding the dynamic response in ferroelectret nanogenerators to enable self-powered tactile systems and human-controlled micro-robots," *Nano Energy*, vol. 63, Sep. 2019, Art. no. 103852.

[38] L. Persano *et al.*, "High performance piezoelectric devices based on aligned arrays of nanofibers of poly(vinylidenefluoride-co-trifluoroethylene)," *Nature Commun.*, vol. 4, Mar. 2013, Art. no. 1633.

[39] V. Nguyen and R. Yang, "Effect of humidity and pressure on the triboelectric nanogenerator," *Nano Energy*, vol. 2, no. 5, pp. 604–608, Sep. 2013.

[40] S. Pence, V. J. Novotny, and A. F. Diaz, "Effect of surface moisture on contact charge of polymers containing ions," *Langmuir*, vol. 10, no. 2, pp. 592–596, Feb. 1994.

[41] E. Németh, V. Albrecht, G. Schubert, and F. Simon, "Polymer triboelectric charging: Dependence on thermodynamic surface properties and relative humidity," *J. Electrostatics*, vol. 58, nos. 1–2, pp. 3–16, May 2003.

Yunqi Cao received the B.S. degree in physics from Wuhan University, Wuhan, Hubei, China, in 2012, and the M.S. degree in materials science and engineering from the University of Florida, Gainesville, FL, USA, in 2014. He is currently pursuing the Ph.D. degree with the Department of Electrical and Computer Engineering, Michigan State University, East Lansing, MI, USA.

In 2015, he was an Etching Process Engineer in the Technology Research and Development Department at Semiconductor Manufacturing International Corporation (SMIC). His current research interests include smart materials based MEMS resonators, microfluidic devices, flexible electronics, and energy harvesting systems.

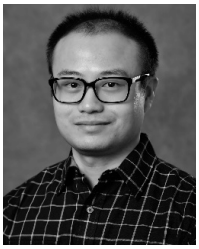

Wei Li received the B.S. and Ph.D. degrees in mechanical engineering from Huazhong University of Science and Technology, China, in 2008 and 2013, respectively, and the second Ph.D. degree from Michigan State University, MI, USA, in 2017. He worked as a Postdoctoral Scholar at the University of California, Berkeley, CA, USA, since 2017. He served as an R&D Engineer at Shanghai Micro Electronics Equipment Co., Ltd., China, and Seagate Technology, USA. His current research interests include MEMS, nanotechnology, smart materials, energy harvesting, and mechatronics. He has published eight patents.

Dr. Li is a member of the IEEE Robotics and Automation Society.

Nelson Sepúlveda (S'05–M'06–SM'11) received the B.S. degree in electrical and computer engineering from the University of Puerto Rico, Mayagüez, Puerto Rico, in 2001, and the M.S. and Ph.D. degrees in electrical and computer engineering from Michigan State University, East Lansing, MI, USA, in 2002 and 2005, respectively.

He has participated in several visiting faculty positions at the National Laboratories. He is currently an Associate Professor with the Electrical and Computer Engineering Department, with a courtesy appointment in the Mechanical Engineering Department, Michigan State University.

Prof. Sepúlveda is a recipient of the NSF CAREER (2010), the MSU Teacher-Scholar Award (2015), the Withrow Excellence Awards (2018), and the Marie Sklodowska-Curie Actions Seal of Excellence (2019).